CHEMISTRY
A EUROPEAN JOURNAL

DOI: 10.1002/chem.200500883

Conducting Poly(aniline) Nanotubes and Nanofibers: Controlled Synthesis and Application in Lithium/Poly(aniline) Rechargeable Batteries

Fangyi Cheng,[a] Wei Tang,[a] Chunsheng Li,[a] Jun Chen,*[a] Huakun Liu,[b] Panwen Shen,[a] and Shixue Dou[b]

Abstract: The primary aim of this work was to synthesize aligned perchloric-acid-doped poly(aniline) ($HClO_4$-doped PANI) nanotubes by a simple alumina template method and to investigate their application in lithium/poly(aniline) rechargeable batteries. Powder X-ray diffraction analysis (XRD), scanning electron microscopy (SEM), transmission electron microscopy (TEM), and Fourier transform infrared (FTIR) analysis were used to characterize the nanostructures obtained. The second aim addressed the preparation of $HClO_4$-doped PANI microspheres and nanofibers on a large scale through a modified spraying technique, since the template synthesis has limitations in mass production. The present synthesis methods are simple and can be extended to the preparation of a broad range of one-dimensional conductive polymers. Furthermore, electrochemical measurements showed that the as-prepared $HClO_4$-doped PANI nanotubes exhibit better electrode performances than their commercial counterparts because they possess more active sites, higher conductivity, and relative flexibility. This indicates that $HClO_4$-doped poly(aniline) nanomaterials are promising in the application of lithium/polymer rechargeable batteries.

Keywords: conducting materials · electrochemistry · nanostructures · polymers · template synthesis

Introduction

Among the family of conjugated conducting polymers, poly(aniline) (PANI) is unique because of its promising chemical, electrical, and optical properties along with its particular redox character.[1,2] Applications of PANI materials are largely based on PANI morphology and the controlled synthesis of it. Nowadays, one-dimensional (1D) PANI nanotubes, nanowires, and nanofibers have attracted considerable attention due to their potential applications in a variety of fields, including molecular electronics, materials science, and biomedical sciences.[3] The synthesis of 1D nanostructures has been aided by templates that act as structural directors.[4,5] Structural directors employed to prepare PANI nanostructures include "soft templates" such as surfactants,[6] inorganic acid,[7] or complex organic doping agents[8] that assist in the self-assembly process, and "hard templates" such as zeolites,[9] and porous alumina membranes,[10] where 1D nanochannels promote the growth of nanotubes or nanowires. Recently, Huang and co-workers developed a general chemical route to synthesize poly(aniline) nanofibers by using interfacial polymerization at an aqueous/organic interface.[11,12] Chiou and co-workers also reported the preparation of poly(aniline) nanofibers by dilute polymerization.[13]

Typically, poly(aniline) has two forms, emeraldine base and emeraldine salt, with a different degree of doping.

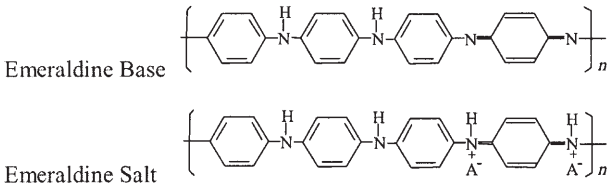

The electrically conductive form of PANI (the emeraldine salt) protonates the imine nitrogen on the polymer backbone and induces charge carriers. When fully doped with a strong acid, the electrical conductivity of PANI greatly increases compared to its undoped (emeraldine base) form.[14] The key parameter for numerous potential applications of

[a] F. Cheng, W. Tang, C. Li, Prof. J. Chen, Prof. P. Shen
Institute of New Energy Material Chemistry
Nankai University, Tianjin 300071 (P. R. China)
Fax: (+86) 22-2350-9118
E-mail: chenabc@nankai.edu.cn

[b] Prof. H. Liu, Prof. S. Dou
Institute for Superconducting and Electronic Materials
University of Wollongong, New South Wales 2522 (Australia)

poly(aniline), for example, in electronics, energy storage, and chemical sensing, is its electrical conductivity. Since the conductivity of PANI depends on its morphology, the acidity of the doped acid, plus the degree of doping,[15] it is reasonable to assume that aligned 1D nanostructured perchloric-acid-doped poly(aniline) ($HClO_4$-PANI) could improve performance compared with common commercial PANI powders.

On the other hand, rechargeable lithium batteries are one of the most actively developed batteries and are becoming more and more important at both fundamental and applied levels.[16] An important application of electroconductive polymers is in rechargeable Li batteries. Although the specific charge–discharge capacities of Li/PANI batteries are relatively low, they have some outstanding characteristics compared with conventional Li batteries such as longer cycle life, lower self-discharge rate, resistance to overdischarge, low manufacturing cost, shape flexibility, and a smaller weight with a higher specific energy.[17] These advantages make the Li/PANI batteries appropriate for application in back-up power sources or in small electronic devices. Thus, increasing the specific capacity of Li/PANI batteries is of great significance to overcome their disadvantages.

It has been demonstrated by different groups that the performance of rechargeable lithium batteries is improved by employing nanosized or, especially, 1D nanostructured active materials because nanostructured materials have high surface areas and possibly enable faster diffusion kinetics for Li ions in electrodes.[18–20] Therefore, in this paper, we report on the synthesis of conducting poly(aniline) nanotubes/nanofibers through an alumina template route and a modified spraying technique. The as-prepared nanostructured $HClO_4$-PANI was further employed as the cathode-active material of rechargeable Li/PANI cells. We found that the nanostructured $HClO_4$-PANI exhibits better performance than that of the alternative commercial powders. The results should foster the application of 1D $HClO_4$-PANI nanostructures in rechargeable Li/polymer batteries.

Results and Discussion

Synthesis of $HClO_4$-PANI nanotubes/nanofibers: At first, a template method was used to study the possibility of preparing 1D conducting PANI nanostructured materials. The templates employed were anodic aluminum oxide (AAO) membranes that had a cylindrical pore structure with a uniform pore diameter of about 200 nm and a membrane thickness of around 60 μm. Figure 1 shows the schematic depiction of the template synthesis process. In the template synthesis, commercial soluble $HClO_4$-PANI powders were used as the

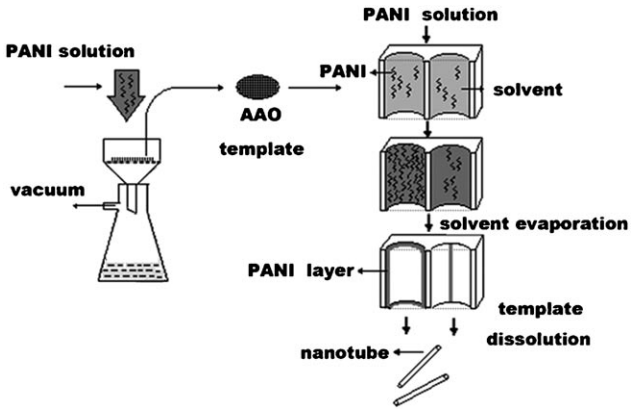

Figure 1. Schematic diagram showing the porous-alumina-template synthesis of $HClO_4$-doped PANI nanotubes.

starting material, and polymer solution penetrated into the template pores from the upper surface of the membrane. At the same time, a vacuum was applied (by using an aspirator) until the solution was pulled through the membrane. After the evaporation of the solvent, the membrane was taken out and dissolved in acid solution to remove the alumina and to free the nanotubes that had been deposited within the pores.

The morphology of the as-synthesized product was characterized by scanning electro microscopy (SEM). Figure 2

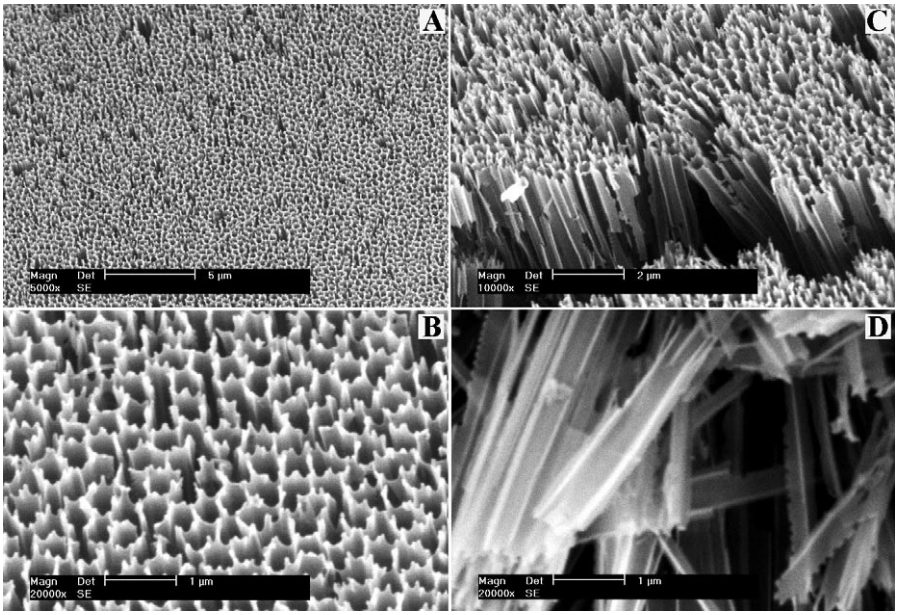

Figure 2. SEM images of the $HClO_4$-doped PANI nanotubes in ordered alignment: A) typical overall view of the tips showing the comb-like structure; B) top view at high magnification; C) side view showing the walls of the tubes; D) vertical cross-section of the tubes after ultrasonic treatment.

shows the typical SEM images of the PANI nanostructures prepared by the template method. As seen in Figure 2 A, copious quantities of $HClO_4$-PANI nanotubes in ordered alignment were obtained. Figure 2 B shows the top view of the nanotube array. The tubes are linked one by one with wall-sharing and possess sawtooth-shaped open ends with long-range hexagonal order. Figure 2 C is the side view of the nanotubes, showing the walls of the tubes that are arranged parallel to each other with smooth surfaces. The average diameter of the tubes is around 300 nm, and larger than the pore diameter of the AAO template. After ultrasonic treatment, the alignment of the as-prepared nanotubes was broken up into dispersive spatulate nanofibers with smooth inner surfaces (Figure 2 D). These observed characteristics of the product can be reasonably understood from the formation mechanism of PANI nanotubes that is in some ways similar to the wetting synthesis reported by Steinhart and co-workers.[21]

In our template synthesis, the low-viscosity polymer precursors ($HClO_4$-doped PANI solution) spread to form a thin film that covers the pore walls of the template in the initial stages of the process because the cohesive driving forces for complete filling are weaker than the adhesive forces. The solution tends to cover the pore walls and forms a homogeneous film with a thickness of several tens of nanometers. As the pores of the template are well-defined, the highly ordered nanotube array is preserved after solvent evaporation. It should be noted that the diameters of the aligned tubes are larger than the pore diameters of the template, probably due to the Barus effect related to elastic memory and elastic recovery. In solution, the polymer molecules usually coil up in an almost random fashion, however, in the pores of the template (as one kind of capillary) there is considerable molecular uncoiling leading to the orientation because of the axial pressure in the sprayer system. When the template is removed, the Brownian movement causes the chain randomization to continue leading to a possible lateral expansion of the tubes. In addition, in long capillaries, swelling occurs as a consequence of the recoverable shear strain that corresponds to the shear stress on the wall after the confinement was removed. As a result, enlarged diameters of the tubes are observed. Furthermore, we can use the Barus effect presented here to interpret the phenomenon of wall-sharing that is observed in the alignment of the nanotubes obtained.

The above results show that $HClO_4$-doped PANI nanotubes can be indeed obtained, however, the alumina-template synthesis is limited in practical application because the product is only obtained on a small scale. Thus a large-scale synthesis of conducting PANI 1D nanostructures is still required. Since the spray technique has been reported to be an effective method to prepare inorganic microspheres and nanowires,[22] a modified spray technology was then further applied to synthesize conducting polymer on a large scale.

Figure 3 shows the experimental set-up for the spray synthesis of conducting PANI, somewhat like squeezing the paste into balls (without steel mesh) or noodles (with steel mesh). Thus $HClO_4$-doped PANI of different morphology can be obtained with or without the utilization of steel mesh that acts as a kind of "template" (obviously different from the AAO membranes).

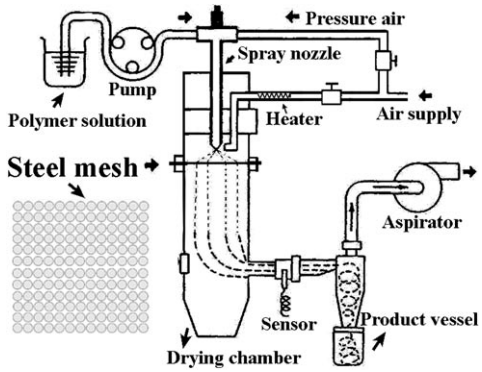

Figure 3. Schematic depiction of the large-scale synthesis of $HClO_4$-PANI nanofibers through a spray technique.

Figure 4 shows the SEM images of the as-prepared product of different morphology. Without the use of steel mesh,

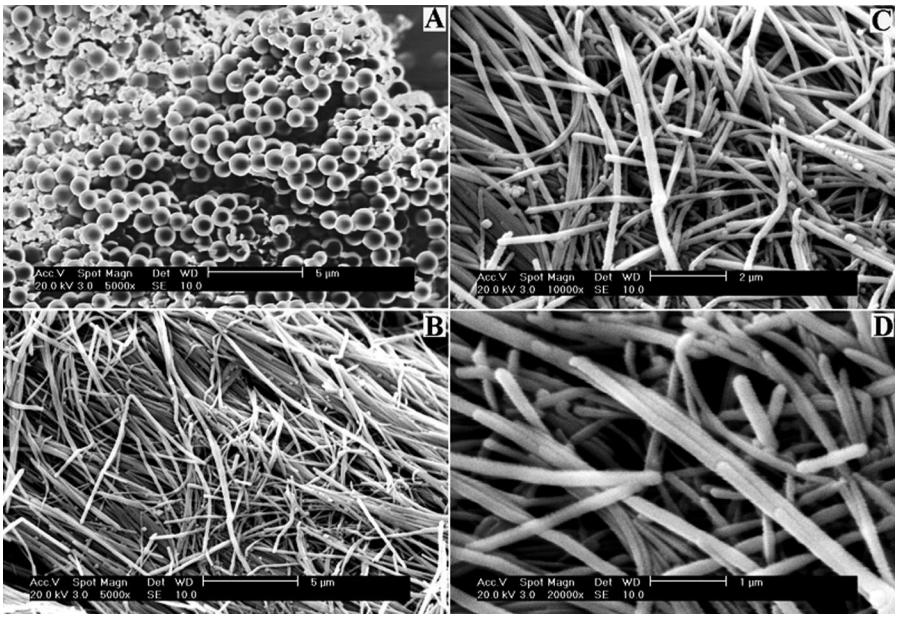

Figure 4. SEM images of the $HClO_4$-doped PANI synthesized through the spray technique: A) without; and B, C, D) with the use of steel mesh at different magnifications.

doped PANI microspheres with average diameters of about 1 μm are obtained (Figure 4 A), somewhat similar to the formation of nickel hydroxide microspheres.[22a] As a comparison, nanofibers can be obtained when using the steel mesh. As seen in Figure 4 B–D, the obtained nanofibers display smooth surfaces, have diameters of 100–200 nm, and lengths of several micrometers. The formation of doped PANI nanowires could be briefly described as follows. After spraying out from the nozzle, the polymer solution was split into tiny droplets with diameters of 1–2 μm that then passed through the steel mesh with the aid of compressed air. Several pieces of steel mesh were piled up together in order to provide enough strength to withstand the impact of spraying. In the drying chamber, the solvent was evaporated quickly when the aspirator was operated; thus the polymer solution became more concentrated and stickier. Penetration of the viscous polymers through the pores of the steel mesh by pushing (from the compressed air) and pulling (by use of the aspirator) led to the formation of nanofibers in a similar way to the extrusion of plaster from tiny pores.

Therefore, 1D $HClO_4$-doped PANI nanostructures of different morphology could be prepared through a template route (obtaining aligned nanotubes) and a spray technique (obtaining nanofibers on a large scale). These two synthesis methods might be applicable to any melt-processible polymer or any conducting polymer that can be dissolved in a solvent. Further study on the as-prepared nanofibers will be carried out. We next focus on the structural characterization and electrochemical investigation of the aligned doped PANI nanotubes that were prepared by the template method.

Structural characterization of the obtained nanotubes: Fourier transform infrared (FTIR) spectra and X-ray diffraction (XRD) patterns were examined to determine the structure of the as-prepared doped PANI nanotubes. Figure 5 shows the FTIR spectra of commercial $HClO_4$-PANI powders and the as-prepared nanotubes obtained by dissolving the AAO template in acid solution. As seen in this figure, the three spectra are almost identical to each other indicating that the molecular structure of the PANI remained unchanged during the preparation process, and that the acid solution used for dissolving the alumina did not influence the structure of the product. The absorbances at about 1590 and 1495 cm^{-1} indicate the signature of the PANI backbone, due to the stretching modes of the protonated quinoid ring and the benzenoid ring. The characteristic strong peak at 1400 cm^{-1} can be assigned to the stretching vibration of the aromatic ammonium group. In addition, the absorbance at 1140 cm^{-1} corresponds to the C=N stretch of the protonated quionoid ring.[23] Hence, the FTIR result reveals that the obtained product keeps the same chemical structure as the starting material ($HClO_4$-doped PANI) and exists in the conducting emeraldine form. In particular, it should be noted that the intensity of the band at 1140 cm^{-1} due to the sample increases compared to that of the commercial powders. The band at 1140 cm^{-1} is considered to be a characteristic peak verifying PANI conductivity.[24] Thus it may suggest that the obtained doped PANI possesses increased conductivity in agreement with our conductivity measurement that will be discussed later.

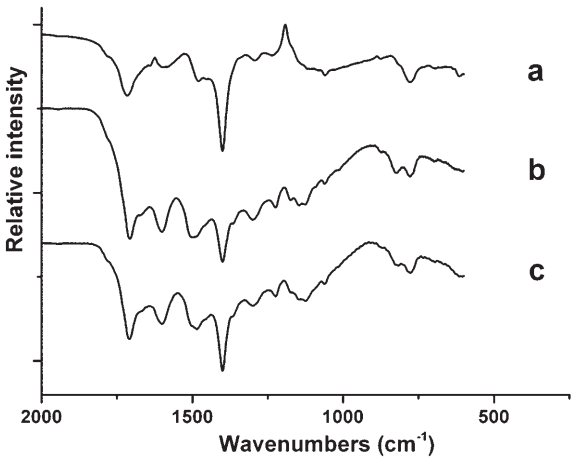

Figure 5. FTIR spectra of commercial $HClO_4$-PANI powders (a), and $HClO_4$-PANI nanostructures obtained by dissolving the alumina template in HCl solution (b), and H_2SO_4 solution (c).

The XRD pattern of the as-prepared product is given in Figure 6. Four broad bands were observed, two of which were present as strong peaks, showing that the resulting doped PANI was partly amorphous and partly crystalline. The first broad band (at $2\theta = 8.9°$) is attributed to the repeat unit of the poly(emeraldine) chain. The peak centered at $2\theta = 20°$ can be ascribed to the periodicity parallel to the polymer chain, while the peak at $2\theta = 25.1°$ may be caused by the periodicity perpendicular to the polymer chains of doped PANI.[25] The reason for the broad band centered at $2\theta = 15°$ is not clear, but presumably, it may be due to the dopant.

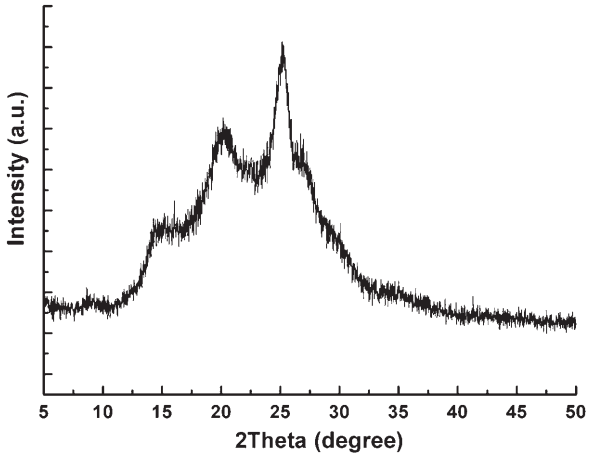

Figure 6. XRD pattern of the as-synthesized $HClO_4$-PANI nanostructures.

Electrochemical measurement of Li/PANI batteries made with the $HClO_4$-PANI nanotubes: Since XRD and FTIR spectra indicated that the PANI nanotubes were prepared with enhanced molecular and supermolecular order, we expected better conductivity for the 1D nanostructured polymer material. The electrical conductivity of the as-synthesized and the commercial doped PANI was measured by a standard four-probe method. Electrical conductivity of the commercial powders was $1.2\,S\,cm^{-1}$, whereas it was $7.1\,S\,cm^{-1}$ for the nanostructures, with an almost sixfold enlargement. This increase in conductivity verified the ordered structure and indicated the superior electrochemical performance of the nanotubes. Hence, the as-prepared $HClO_4$-PANI nanotubes were employed as positive electrode material for Li/PANI rechargeable cells.

Figure 7 shows the cyclic voltammograms (CV) for the electrode made with the doped PANI nanotubes, and the electrode composed of commercial powders for comparison. Ten cycles were measured, but only the second cycle is shown here, since the first cycle of voltammograms was not steady and the subsequent cycles 3–10 remained nearly the same as the second one. It can be seen that, for the nanotube electrode, the corresponding cathodic and anodic peaks are relatively stronger than those of the electrode made with commercial powders, although they both present related broad peaks centered at the same positions. These stronger peaks may indicate that as the active cathode material of Li/PANI secondary batteries, the redox activity of the $HClO_4$-doped PANI nanotubes is much greater than that of the commercial powders. It should also be noted that the corresponding cathodic and anodic areas of nanotube electrodes are much larger than the counterpart powders during the cyclic process that is an indication of improved charge–discharge capacities.

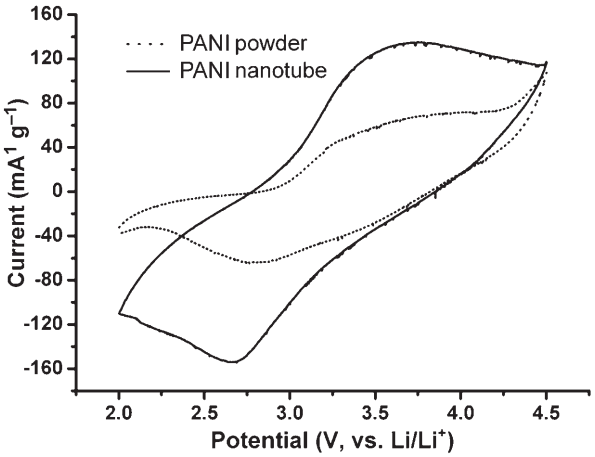

Figure 7. Cyclic voltammograms of the electrodes made with doped PANI nanotubes (——) and commercial powders (•••••). Temperature: 25 °C; scan rate: 1 mV s^{-1}.

Charge–discharge measurements were taken to further investigate the capacity and cycling capability of the Li/PANI rechargeable cells constructed with the as-prepared nanostructured doped PANI or the commercial powders. Figures 8 and 9 show the charge–discharge curves for the Li/PANI cells made with doped PANI commercial powders and nanostructured doped PANI, respectively.

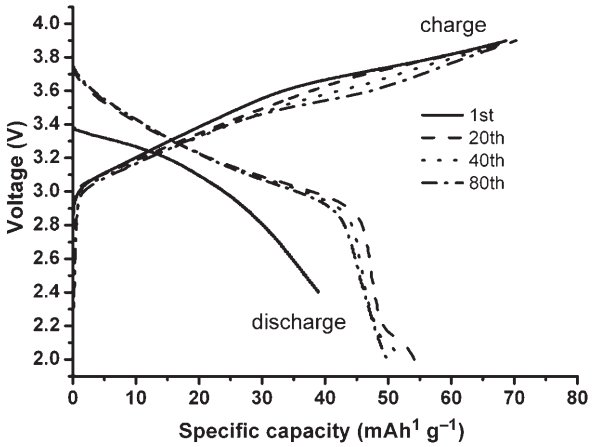

Figure 8. Charge–discharge cycling performances of the Li/PANI cell composed of commercial doped PANI powders at the constant charge/discharge current density of 20 mA g^{-1} and the temperature of 25 °C.

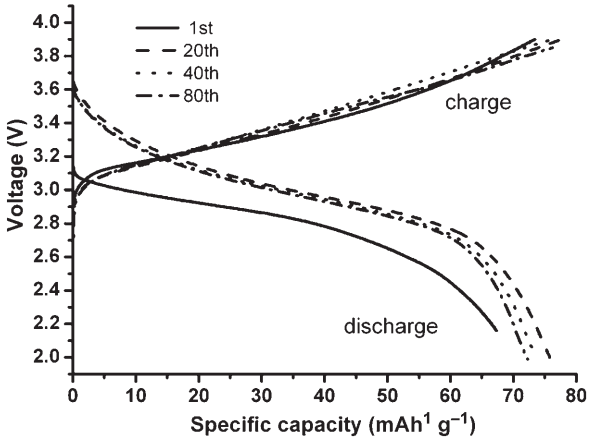

Figure 9. Charge–discharge cycling performances of Li/PANI cells made with doped PANI nanotubes at the constant charge/discharge current density of 20 mA g^{-1} and the temperature of 25 °C.

As seen in Figures 8 and 9, the first discharge curves are very different from the subsequent ones. This difference may be due to the gradual activation in the first discharge process that is also observed in the CV measurement. The PANI electrode might have undergone a course from unstable state to stable state, after which, the charge–discharge curves became steady and showed good reversibility with an average discharge-plateau voltage of 3.0 V plus an average charge-plateau voltage of 3.4 V. The reaction of Li/PANI batteries was reported as given in Equation (1).[26]

$$\text{emeraldine base} + 2\,LiClO_4 \underset{\text{discharge}}{\overset{\text{charge}}{\rightleftharpoons}} 2\,Li + \text{emeraldine salt} \quad (1)$$

Based on the above reaction, the theoretical specific capacity of emeraldine salt ($HClO_4$-doped PANI) is 147 $mA\,h\,g^{-1}$ referring to the PANI weight alone, in contrast to 95.2 $mA\,h\,g^{-1}$ calculated by including the weight of ClO_4^-. The values of specific capacity and specific energy in this study were obtained considering the weights of PANI as well as ClO_4^-.

For the two constructed Li/PANI cells, the discharge and charge capacity gradually increased with the number of charge–discharge cycles, and reached a maximum in the twentieth cycle that we believed to be due to the electrolyte progressively penetrating into the polymer.[27] The highest practical discharge capacity of the commercial doped PANI powders is 54.2 $mA\,h\,g^{-1}$, only 57% of the theoretical capacity, that is comparable with the values reported in literature.[17,28] In contrast, the corresponding value for the doped PANI nanotubes/nanofibers reaches 75.7 $mA\,h\,g^{-1}$, attaining about 80% of the theoretical capacity. Thus, the discharge capacity of the nanostructured PANI is much higher than that of the commercial PANI powders. Meanwhile, a specific discharge energy of 227 $W\,h\,Kg^{-1}$ is found for the nanostructures, showing their storage ability of high specific energy. We also find from Figure 9 that the discharge capacity of the nanotubes in the 80th cycle is 72.3 $mA\,h\,g^{-1}$, retaining 95.5% of the obtained highest discharge capacity. The average capacity deterioration of the nanostructured doped PANI is less than 0.05 $mA\,h\,g^{-1}$ for one cycle, indicating its superior cycling capability. In addition, the nanotube electrode exhibits longer charge and discharge plateaux than the electrode composed of commercial powders. Furthermore, for the nanotube/nanofiber electrode, the Coulombic efficiency of the 20th charge–discharge cycle and the 80th cycle is 97.5% and 94.9%, respectively. Accordingly, the utilization efficiency of doped PANI nanotubes as cathode-active material for Li/PANI rechargeable batteries is quite high.

From the above CV and charge–discharge measurements, we can see that the as-prepared $HClO_4$ doped PANI nanotubes show better cycling capability, larger charge–discharge capacities, and higher utilization efficiency than the commercial powders. This improved performance may result from the following aspects. First, the as-prepared $HClO_4$-doped PANI nanotubes possess higher specific surface areas compared to commercial powders due to their small size, and they can offer more active sites for the reaction between electrolyte and electrode material. The 1D tubular structure also favors the diffusion of ions that occurs in the charge–discharge process since diffusion can take place through both sides of the tube walls (Figure 10). Second, the electrode properties are related to the higher conductivity of the nanotubes over the commercial powders, leading to faster electronic kinetics and lower internal resistance for the electrode reactions. Third, the ordered nanotube alignment is relatively flexible, thus the tubular structure is able to stand the repeated lithium intercalation–deintercalation during charge–discharge cycles. As a result, improved electrochemical performance can be reasonably understood to some extent. Our future work will obtain more evidence through various techniques to further explore the reasons for the superior performance of the 1D doped PANI nanostructures.

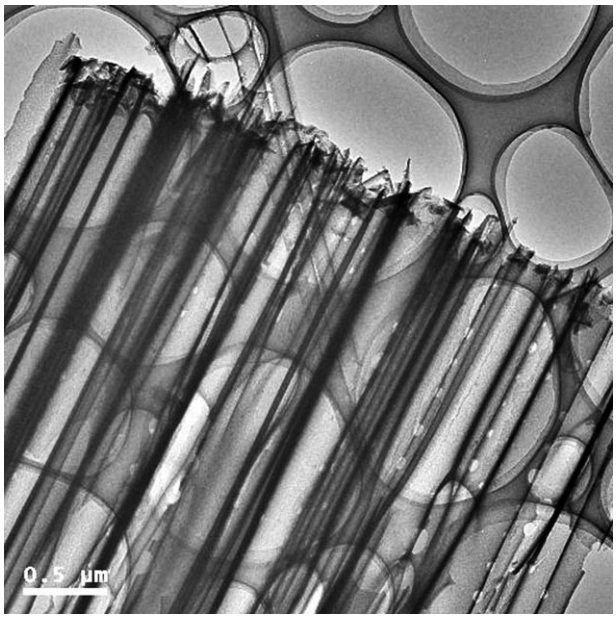

Figure 10. TEM image of the $HClO_4$-doped PANI nanotubes in ordered alignment.

Conclusion

Conducting $HClO_4$-doped poly(aniline) nanotubes and nanofibers have been prepared through a template route and a spray technique, respectively. The present method can be extended to the synthesis of any 1D nanostructured conducting polymer which is melt-processible or solvent-soluble. In addition, we found that the as-prepared $HClO_4$-doped poly(aniline) nanotubes exhibit higher electrical conductivity, larger charge–discharge capacity, and better cycling capability than the commercial doped PANI powders. The results of the electrochemical measurements showed the promising application of the doped PANI nanostructures in Li/PANI rechargeable batteries. The reason for the improved electrochemical performance has been preliminarily discussed with regards to more active sites, higher conductivity, and relatively flexible tubular structure. Further study will be carried out to elucidate the electrochemical behavior of the 1D nanostructured $HClO_4$-doped PANI.

Experimental Section

Materials: All the chemicals were of analytical grade and were used as received without further purification. De-ionized water was used throughout. Conducting perchloric-acid-doped poly(aniline) (doping level: $[Cl]/[N] \approx 0.5$; average particle-size: 15 μm) and N-methylpyrrolidinone (NMP) were supplied by Chengdu Organic Reagent Company, P. R. China. Anodic aluminum oxide membranes were purchased from Whatman (∅ 47 mm with quoted pore-diameters of 200 nm).

Methods: The conducting $HClO_4$-PANI nanotubes were prepared by a simple template method, as shown in Figure 1. In a typical synthesis, doped poly(aniline) (4.082 g) was dissolved in *N*-methylpyrrolidinone (20 g) with magnetic stirring for 4 h at 50 °C to obtain a homogeneous solution. The $HClO_4$-PANI solution was placed on the top side of the template membrane and wetted the pores of the AAO membrane. A vacuum was then employed to pull the polymer solution through the membrane and to evaporate the solvent. The resulting membrane was dissolved in HCl (2 M) or H_2SO_4 (1 M) solution to free the polymer within it. The obtained solid was filtered, washed with distilled water, and was dried in air.

Doped PANI nanofibers were prepared through a spray technique with a modified minispray (Yamato, Model GA-32), as shown in Figure 3. Polymer solution ($HClO_4$-PANI dissolved in NMP, concentration about 20 wt %) was pulled through the sample inlet by the fluid pump and was transported to the outlet of the spray nozzle by compressed air. Air was used for carrying the reaction reagent and to control the system temperature. After emerging from the outlet of the spray nozzle, the polymer solution penetrated into the pores of the steel mesh (3–5 pieces piled up together that could be easily placed and replaced through the upper side of the drying chamber). At the same time, a vacuum was applied (by using an aspirator) to pull the solution through the membrane and to evaporate the solvent. The product was collected in the product vessel, and was washed and dried for further investigation.

Characterization: The scanning electron microscopy (SEM) images were taken on a Philips XL-30 SEM with accelerating voltage of 20 kV. Transmission electron microscopy (TEM) analysis was carried out on a Philips Tecnai F20 TEM instrument operating at 200 kV. X-ray diffraction (XRD) patterns were obtained with a Rigaku D/max 2500 X-ray diffractometer ($Cu_{K\alpha}$ radiation, $\lambda = 1.5418$ Å). The Fourier transform infrared (FTIR) spectra were obtained on a Bruker Tensor 27 spectrometer in the range of 500–2000 cm^{-1} on sample pellets made with KBr.

Electrochemical measurement: The electrical conductivity of the commercial doped PANI powders and the as-prepared nanostructures was measured at room temperature by using a standard four-probe method (Keithley 2400 SourceMeter) with an error of less than 5%. Electrochemical measurements were carried out using two-electrode cells with lithium metal as the counter electrode. The working electrodes were fabricated by compressing the mixture of 80 wt % active materials, 15 wt % acetylene black, and 5 wt % poly(tetrafluoroethylene) onto a nickel foam. The cell assembly was operated in a glovebox filled with pure argon (99.999 %) in the presence of an oxygen scavenger and a sodium drying-agent. The electrolyte solution was $LiClO_4$ (0.5 M) dissolved in a mixture of propylene carbonate (PC) and dimethyl carbonate (DMC) with the volume ratio of PC/DMC = 1:1. Electrochemical performance was investigated by using a Solartron SI 1260 Potentiostat Analyzer with a 1287 Interface and a modified Arbin charge–discharge unit. Cyclic voltammograms were measured at a scan rate of 1 $mV\,s^{-1}$ at 25 °C. Charge–discharge cycles were tested with a constant current density of 20 $mA\,g^{-1}$ in the potential range 2.0–3.9 V. All the voltages are reported in this paper versus Li/Li^+. The discharge capacities of the PANI electrodes were based on the amount of the active material PANI that excludes the weight of acetylene black and poly(tetrafluoroethylene) mixed in the electrode.

Acknowledgements

This work was supported by the National NSFC (20325102) and National Key Basic Research Program (2005CB623607).

[1] a) T. A. Skotheim, R. L. Elsenbaumer, J. R. Eeynolds, *Handbook of Conducting Polymers*, 2nd ed., Marcel Dekker, New York, **1998**; b) H. Shirakawa, *Angew. Chem.* **2001**, *113*, 2642; *Angew. Chem. Int. Ed.* **2001**, *40*, 2574; c) A. G. MacDiarmid, *Angew. Chem.* **2001**, *113*, 2649; *Angew. Chem. Int. Ed.* **2001**, *40*, 2581; d) A. J. Heeger, *Angew. Chem.* **2001**, *113*, 2660; *Angew. Chem. Int. Ed.* **2001**, *40*, 2591.
[2] a) A. G. MacDiarmid, J. C. Chiang, A. F. Richter, *Synth. Met.* **1987**, *18*, 285; b) Y. Cao, P. Smith, A. J. Heeger, *Synth. Met.* **1992**, *48*, 91; c) S. W. Ng, K. G. Neoh, J. T. Sampanthar, E. T. Kang, K. L. Tan, *J. Phys. Chem. B* **2001**, *105*, 5618.
[3] a) H. S. Nalwa, *Handbook of Organic Conductive Molecules and Polymers*, Wiley, Chichester, **1997**; b) S. Choi, S. Park, *Adv. Mater.* **2000**, *12*, 1547; c) J. Liu, Y. H. Lin, L. Liang, J. A. Voigt, D. L. Huber, Z. R. Tian, E. Coker, B. McKenzie, M. J. McDermott, *Chem. Eur. J.* **2003**, *9*, 605.
[4] M. Wirtz, M. Parker, Y. Kobayashi, C. R. Martin, *Chem. Eur. J.* **2002**, *8*, 3573.
[5] F. Schüth, *Angew. Chem.* **2003**, *115*, 3730; *Angew. Chem. Int. Ed.* **2003**, *42*, 3604.
[6] a) A. D. W. Carswell, E. A. O'Rear, B. P. Grady, *J. Am. Chem. Soc.* **2003**, *125*, 14793; b) L. Yu, J. I. Lee, K. W. Shin, C. E. Park, R. Holze, *J. Appl. Polym. Sci.* **2003**, *88*, 1550.
[7] Z. X. Wei, L. J. Zhang, M. Yu, Y. S. Yang, M. X. Wan, *Adv. Mater.* **2003**, *15*, 1382.
[8] H. J. Qiu, M. X. Wan, B. Mattews, L. M. Dai, *Macromolecules* **2001**, *34*, 675.
[9] C. G. Wu, T. Bein, *Science* **1994**, *264*, 1757.
[10] C. R. Martin, *Acc. Chem. Res.* **1995**, *28*, 61.
[11] J. Huang, S. Virji, B. H. Weiller, R. B. Kaner, *Chem. Eur. J.* **2004**, *10*, 1314.
[12] J. Huang, R. B. Kaner, *Angew. Chem.* **2004**, *116*, 5941; *Angew. Chem. Int. Ed.* **2004**, *43*, 5817.
[13] N. R. Chiou, A. J. Epstein, *Adv. Mater.* **2005**, *17*, 1679.
[14] W. S. Huang, B. D. Humphrey, A. G. MacDiarmid, *J. Chem. Soc. Faraday Trans.* **1986**, *82*, 2385.
[15] A. R. Hopkins, R. A. Lipeles, W. H. Kao, *Thin Solid Films* **2004**, *447–448*, 474.
[16] a) D. Linden, T. B. Reddy, *Handbook of Batteries*, 3rd ed., McGraw–Hill Inc., New York, **2002**; b) J. M. Tarascon, M. Armand, *Nature* **2001**, *414*, 359.
[17] K. S. Ryu, K. M. Kim, S. G. Kang, G. J. Lee, S. H. Chang, *Solid State Ionics* **2000**, *135*, 229.
[18] a) M. Nishizawa, K. Mukai, S. Kuwabata, C. R. Martin, H. Yoneyama, *J. Electrochem. Soc.* **1997**, *144*, 1923; b) G. Che, B. B. Lakshmi, E. R. Fisher, C. R. Martin, *Nature* **1998**, *393*, 346.
[19] a) P. R. Bueno, E. R. Leite, *J. Phys. Chem. B* **2003**, *107*, 8868; b) P. R. Bueno, E. R. Leite, T. R. Giraldi, L. O. S. Bulhões, E. Longo, *J. Phys. Chem. B* **2003**, *107*, 8878.
[20] a) J. Chen, L. N. Xu, W. Y. Li, X. L. Gou, *Adv. Mater.* **2005**, *17*, 582; b) X. X. Li, F. Y. Cheng, B. Guo, J. Chen, *J. Phys. Chem. B* **2005**, *109*, 14017.
[21] M. Steinhart, J. H. Wendorff, A. Greiner, R. B. Wehrspohn, K. Nielsch, J. Schilling, J. Choi, U. Gösele, *Science* **2002**, *296*, 1997.
[22] a) J. Chen, D. H. Bradhurst, S. X. Dou, H. K. Liu, *J. Electrochem. Soc.* **1999**, *146*, 3606; b) S. R. C. Vivekchand, G. Gundiah, A. Govindaraj, C. N. R. Rao, *Adv. Mater.* **2004**, *16*, 1842.
[23] S. Quillard, G. Louarn, S. Lefrant, A. G. MacDiarmid, *Phys. Rev. B* **1994**, *50*, 12496.
[24] J. E. Huang, X. H. Li, J. C. Xu, H. L. Li, *Carbon* **2003**, *41*, 2731.
[25] L. J. Zhang, M. X. Wan, *Adv. Funct. Mater.* **2003**, *13*, 815.
[26] L. L. Yang, W. H. Qiu, Q. G. Liu, *Solid State Ionics* **1996**, *86–88*, 819.
[27] E. M. Geniès, P. Hany, C. Santier, *J. Appl. Electrochem.* **1988**, *18*, 751.
[28] a) P. Novák, K. Müller, K. S. V. Santhanam, O. Haas, *Chem. Rev.* **1997**, *97*, 207; b) W. X. Chen, Z. Xu, L. S. Yang, *J. Power Sources* **2001**, *102*, 112.

Received: July 26, 2005
Revised: December 4, 2005
Published online: January 23, 2006

